Activation of frozen ferroelectric domain wall by magnetic field sweeping in multiferroic $CuFeO_2$

H. Tamatsukuri,* S. Mitsuda, T. Nakajima, K. Shibata, and C. Kaneko
Department of Physics, Faculty of Science, Tokyo University of Science, Tokyo 162-8601, Japan

K. Takehana and Y. Imanaka
National Institute for Materials Science, Nano Physics Group, 3-13 Sakura, Tsukuba, Ibaraki 305-0003, Japan

N. Terada and H. Kitazawa
National Institute for Materials Science, Neutron Scattering Group, 1-2-1 Sengen, Tsukuba, Ibaraki 305-0047, Japan

K. Prokes, S. Matas, K. Kiefer, S. Paeckel, A. Sokolowski, B. Klemke, and S. Gerischer
Helmholtz-Centre Berlin for Materials and Energy, Glienicker Straße 100, Berlin 14109, Germany
(Received 13 October 2015; revised manuscript received 16 March 2016; published 3 May 2016)

In a ferroelectric helimagnetic phase of a spin-driven multiferroic, $CuFeO_2$, we find irreversibly additive evolution of electric polarization P induced by sweeping magnetic field H under an applied electric field E, despite a large coercive electric field in the phase. From the unpolarized neutron diffraction experiments with *in situ* P measurements under applied E, we reveal that increment of P is achieved by the variation of an incommensurate magnetic modulation wave number q of the helical magnetic ordering in H sweeping regardless of increasing or decreasing H. Combining this result with the H dependence of the magnetic diffraction intensity and a result of off-bench P measurements, we conclude that the H evolution of P is caused by a change in a (ferroelectric) helicity domain volume fraction by driving the helicity domain wall (DW). Taking into account the results of further detailed P measurements, we provide a speculation for microscopic helicity DW motion. The present study demonstrates the magnetoelectric cross correlation in driving a multiferroic DW: we can activate the frozen ferroelectric DW by means of H sweeping. This is also an achievement of driving an antiferromagnetic DW, which is difficult in conventional antiferromagnets in principle.

DOI: 10.1103/PhysRevB.93.174101

I. INTRODUCTION

In recent years, many magnetic materials with "spin-driven ferroelectricity" have been reported [1–4]. These materials, known as multiferroics, show a giant magnetoelectric (ME) effect, which is the induction or control of electric polarization by a magnetic field H and vice versa. In these materials, the ferroelectricity often emerges as a result of inversion-symmetry breaking by spiral magnetic structures such as a cycloid or a proper screw. As for the microscopic mechanism related to how these magnetic structures induce ferroelectric polarization P, several theories have been proposed, and the giant ME effect observed for such spin-driven ferroelectric materials has been well explained [5–7]. In general, however, bulk properties depend not only on microscopic magnetic structures but also on semimacroscopic multiferroic domain structures or domain-wall (DW) structures, which are expected to show a novel response to external fields. For example, multiferroic DW motion caused by ac electric field E accounts for magnetically tunable dielectric dispersions in $DyMnO_3$ [8,9]. Also, from the viewpoint of application of multiferroic devices such as nonvolatile memory [10], it is necessary to investigate the multiferroic domain structures or DW structures as well as magnetic structures.

The delafossite compound $CuFeO_2$ (CFO) system investigated here is one of the model materials exhibiting spin-driven ferroelectricity. CFO is known as a typical example of triangular-lattice antiferromagnets, in which magnetic moment is carried by an Fe^{3+} ion ($S = 5/2$). In zero H, successive magnetic phase transitions occur from the paramagnetic (PM) phase to the collinear four-sublattice (4SL) phase ($\uparrow\uparrow\downarrow\downarrow$; $T \leqslant T_{N2} \sim 11$ K), with the magnetic moments along the c axis, through a partially disordered (PD) phase ($T_{N2} \leqslant T \leqslant T_{N1} \sim 14$ K), with a sinusoidally amplitude-modulated magnetic structure having moments along the c axis [11]. When H is applied along the c axis up to 15 T below T_{N2}, two other magnetic phases are realized [12,13]: a ferroelectric-incommensurate magnetic (FE-ICM) phase with a helical magnetic structure (7 T $\lesssim H \lesssim$ 12 T) and a collinear five-sublattice (5SL) phase ($\uparrow\uparrow\uparrow\downarrow\downarrow$) with magnetic moments along the c axis ($H \gtrsim 12$ T). The FE-ICM phase is also realized even under zero H by substituting a few percent of nonmagnetic ions (Al^{3+},Ga^{3+}, or Rh^{3+}) for Fe^{3+} [14–17].

In all of these phases, the magnetic modulation vector is $(q,q,3/2)$. Because of the trigonal symmetry along the c axis, CFO has two other magnetic modulation vectors of $(-2q,q,3/2)$ and $(q,-2q,3/2)$, which are equivalent to $(q,q,3/2)$, resulting in the existence of three magnetic domains. We refer to them as the (110), $(\bar{2}10)$, and $(1\bar{2}0)$ domains, respectively, and collectively call them q domains. In the FE-ICM phase, a helical magnetic structure whose screw axis is parallel to the [110] (or $[\bar{2}10]$, $[1\bar{2}0]$) direction induces ferroelectric polarizations parallel to the [110] (or $[\bar{2}10]$, $[1\bar{2}0]$) direction [18,19], which arise through the d-p hybridization mechanism [7]. Because there is one-to-one correspondence between directions of P and the spin helicity

*tamatsukuri@nsmsmac4.ph.kagu.tus.ac.jp

 ©2016 American Physical Society

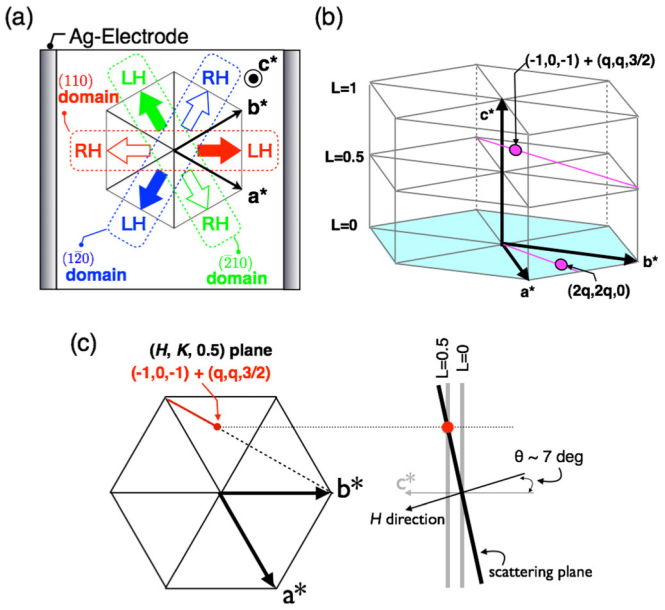

FIG. 1. (a) Schematic illustration of six magnetic domains and the experimental configuration for measurements of P. (b) Locations of the magnetic Bragg points in the reciprocal lattice space. When vertical H is applied along the c axis, the scattering plane is the $(H,K,0)$ plane (light blue shaded area). For visibility, the c^* axis is elongated. (c) Geometrical relationship between the scattering plane and the $(\bar{1},0,\bar{1}) + (q,q,3/2)$ fundamental magnetic Bragg point when the sample is inclined. This Bragg point can be put on the scattering plane by inclining the sample from the c axis (by $\sim 7^\circ$).

(a right-handed or left-handed helical arrangement of spins) [19], each q domain consists of two domains with different helicities. We refer to them as helicity domains. Consequently, six multiferroic domains exist in the FE-ICM phase of CFO, as shown in Fig. 1(a). By taking into account the magnetic domain structure and magnetic structure in the FE-ICM phase, $P_{[110]}$, which is P macroscopically measured by using [110] electrodes, is determined by three factors: (i) the q domain volume fractions, (ii) the helicity domain volume fractions, and (iii) the local electric polarization determined by the helical magnetic structure $P_{\rm local}$. When we use the [110] electrodes, P in the $(\bar{2}10)$ or $(1\bar{2}0)$ domain contributes only half to $P_{[110]}$ because it is projected onto the [110] electrodes by $\cos 60^\circ$, as shown in Fig. 1(a). This is the reason why the value of $P_{[110]}$ is also affected by the change in the q domain volume fractions.

Since CFO systems form such a six-multiferroic domain structure in the FE-ICM phase, novel control of the multiferroic domain volume fraction has been performed. For example, Nakajima *et al.* reported that the increase or decrease of P in the FE-ICM phase of $CuFe_{1-x}Ga_xO_2$ is synchronized with uniaxial pressure via the lattice distortion [20]. Seki *et al.* reported that H rotating within the ab plane causes a 120° flop of P in the FE-ICM phase of $CuFe_{1-x}Ga_xO_2$ [21]. These phenomena were achieved by the rearrangement of q domain structures below the ferroelectric phase-transition temperature. In contrast, the uniaxial pressure is useless for the modification of helicity domain configurations below the ferroelectric phase-transition temperature in this system because the helicity domains have no coupling with the lattice distortion. Also with regard to the magnetic field, for directly driving the helicity DWs, we need to apply the conjugate magnetic field to the order parameter in this system (namely, the magnetic field with the helical magnetic modulation wave vector in the FE-ICM phase). Consequently, only E remains as the practicable external field for driving the helicity DWs. Nevertheless, neither the q DWs nor the helicity DWs are driven by E owing to a large coercive electric field above 1 MV/m at low temperature, even though the nuclei growth of one of the helicity domains at (first-order) ferroelectric transitions can be easily promoted by an applied E [22]. Thus, the rearrangement of helicity domain structures below the ferroelectric phase-transition temperature has not been accomplished yet.

In this paper, we report a peculiarly irreversible H evolution of P induced by H sweeping under applied E in the FE-ICM phase of CFO, which is caused by a change in the helicity domain volume fractions by driving the helicity DWs. Our study demonstrates that a H variation of the incommensurate wave number q can activate the frozen ferroelectric helicity DWs, which is expected to be realized in other spin-driven ferroelectrics as well. This is also an achievement of driving the antiferromagnetic DW through the cross correlation between antiferromagnetism and ferroelectricity. Based on our experimental results, we provide a speculation for microscopic helicity DW motion.

II. EXPERIMENTAL DETAILS

Single crystals of CFO and $CuFe_{1-x}Al_xO_2$ ($x = 0.02$; CFAO) of nominal compositions were prepared using the floating-zone method [23].

A. Electric polarization measurements

Crystals were cut into thin plates ($\sim 3 \times 4 \times 0.26$ mm) with the widest faces perpendicular to the [110] direction. For the electrodes, silver paste was painted onto these surfaces, and E (typically, 800 kV/m) was applied along the [110] axis. H was applied along the c axis using the 15-T superconducting magnet installed at the Tsukuba Magnet Laboratory at the National Institute for Materials Science (NIMS). P was deduced by the time integration of a polarization current (typical peak values are $\sim 1 \times 10^{-11}$ A at 2 K and $\sim 2.5 \times 10^{-11}$ A at 7 K) flowing through changing temperature T or H, which was measured with an electrometer (Keithley 6517A). The typical sweep rate for H was 11.4 mT/s. When E was applied, a leakage current flowed (for example, $\sim 9 \times 10^{-14}$ A at 2 K and $\sim 1 \times 10^{-12}$ A at 7 K) because CFO and CFAO are intrinsic semiconductors. We thus subtracted it from the polarization current before time integration. Unless specifically noted, the data for $P_{[110]}$ were obtained at NIMS.

B. Neutron diffraction experiments

Neutron diffraction measurements were carried out at the two-axis diffractometer E4 at Helmholtz-Zentrum Berlin (HZB). The wavelength of the incident neutron was 2.44 Å. H was applied using the 14.5-T vertical field cryomagnet

VM-1. We employed two diffraction setups for *in situ* $P_{[110]}$ measurements and for measurements of $2q$.

1. Neutron diffraction experiments with in situ electric polarization measurements

The crystal was cut into thin plates ($4.26 \times 5.91 \times 1.06$ mm) with the widest faces perpendicular to the [110] axis. The electrodes consisted of silver paste painted onto these surfaces. P was deduced by the same manner as described above. The polarization currents were measured with an electrometer (Keithley 6517B). Here, we should mention that measurements of polarization currents in these experiments were rather problematic. Because the sample used in the experiments was relatively thick to gain the neutron counts, we needed to apply a high voltage V of approximately 800 V to the sample in order to adapt the magnitude of E to the data obtained at NIMS. When the high voltage, from 400 V ($E \simeq 377$ kV/m) to 1000 V ($E \simeq 943$ kV/m), was applied to the sample, however, we observed an unexpected current, which flowed in the direction inverse to the signal polarization current [Fig. 2(c)]. This nuisance current was conspicuously seen at higher temperatures, especially at 8.5 K, and we could not deduce $P_{[110]}$ at that temperature. The origin of this nuisance current has not yet been determined. When we restricted applied voltage to below 400 V, however, we could obtain the current data without the nuisance current, which qualitatively reproduces the value of $P_{[110]}$ observed previously in $P_{[110]}$ measurements at NIMS.

To provide access to the FE-ICM phase, we need to apply vertical H along the c axis, which means that we can only survey magnetic reflections with spin density projected on the c plane in the $(hk0)$ zone. In addition, the only accessible fundamental $(q,q,0)$ magnetic Bragg reflections are forbidden because the helical spin arrangements in the c plane are stacked antiferromagnetically along the c axis [12]. For this reason, we measured the H dependence of q using $(\bar{1},0,\bar{1}) + (q,q,3/2)$ fundamental magnetic Bragg reflections by inclining the sample from the c axis (by $\sim 7^\circ$) for vertical H [see Fig. 1(c)] [24]. In principle, we need to perform the $(h-1,h,0.5)$ reciprocal lattice scan in order to follow a H variation of the $(q,q,3/2)$ magnetic Bragg point. However, this is difficult in the experimental configuration. Therefore, we have performed a ω scan using the two-dimensional E4 area detector, which covers a wide range of 2θ. Although we cannot deduce the absolute value of q from this scan due to the lack of observable Bragg reflections as a reference, we can detect a peak shift in the scan corresponding to a variation of q, as shown in Fig. 2(a). We can then linearly map the peak shift in the ω scan to the H dependence of q using the H dependence of $2q$ as described below. We have confirmed that the nature of the H dependence of $P_{[110]}$ does not change even by applying a slightly inclined H, although the phase-transition field was slightly modified. The typical rate of H sweeping was 8.67 mT/s.

2. Measurements of 2q

As described above, fundamental $(q,q,0)$ magnetic Bragg reflections are forbidden. Therefore, to obtain the absolute value of q, we have measured the H dependence of $2q$ using the $(2q,2q,0)$-second-harmonic reflections [see Fig. 1(b)] arising from the distortion of the helical magnetic structure in the regular setup. Because we can measure the magnetic reflections from $(-4q,2q,0)$ or $(2q,-4q,0)$ magnetic Bragg points, which are equivalent to the $(2q,2q,0)$ magnetic Bragg point and belong to the other q domains, we can also directly survey the H change in the q domain volume fractions from this experiment. For these measurements, we have used a relatively large sample (~ 1 g). Note that E was not applied in this experiment.

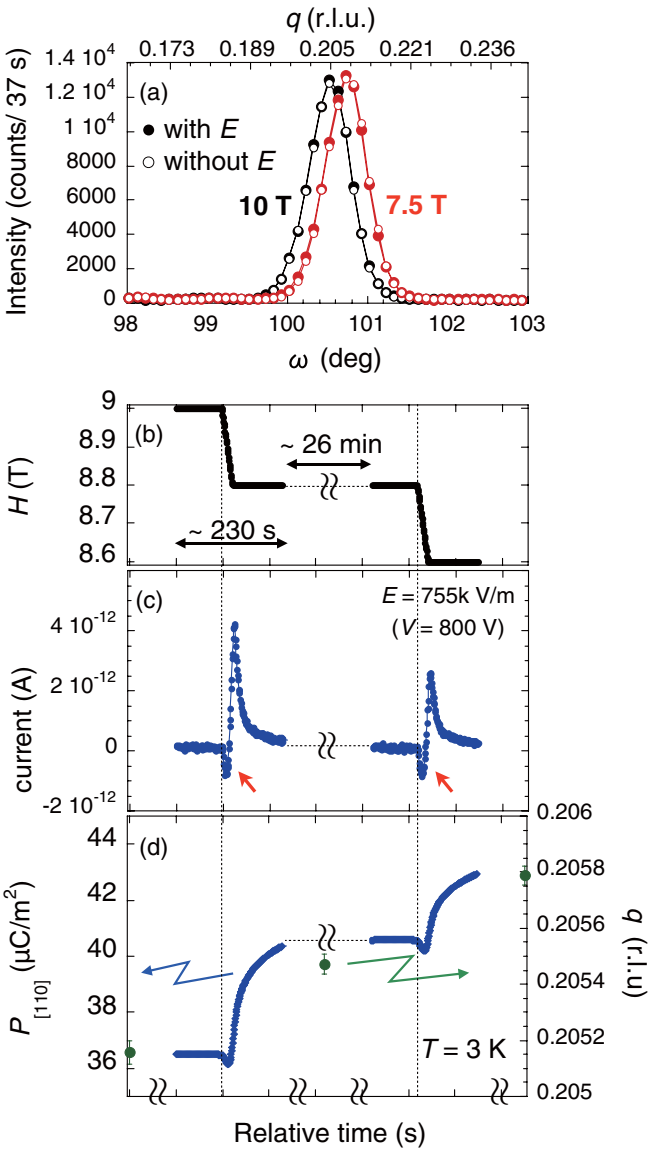

FIG. 2. (a) Typical diffraction profiles at 10 and 7.5 T with and without applied E at 3 K. The upper abscissa shows the q value corresponding to the angle shown in the lower abscissa. These q values are obtained by the linear mapping using the result of $2q$ measurements, as mentioned in Sec. II B 1. (b)–(d) Typical results of the neutron diffraction experiments with *in situ* P measurements from 9 to 8.6 T at 3 K. The change in (b) H, (c) polarization current, and (d) $P_{[110]}$ and q as a function of relative time. The data for the polarization current and $P_{[110]}$ were obtained at HZB. Red arrows in (c) indicate the nuisance current due to an applied voltage V of 800 V.

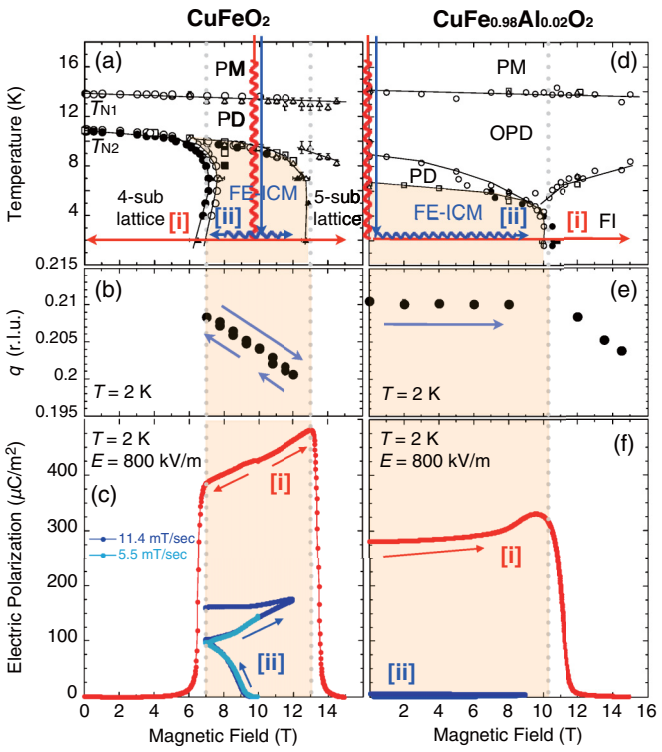

FIG. 3. (a) Measurement paths on the H-T phase diagram for $CuFeO_2$. Wavy lines denote that electric field is applied. In process [i], the polarization current was measured while increasing H to 15 T or decreasing H to 0 from 10 T at 2 K without E. Before the measurements, E_p was applied typically at 16 K on cooling and was removed after cooling down to 2 K. In process [ii], the polarization current was measured with H sweeping in the FE-ICM phase under applied E at 2 K after cooling without E_p at 10 T. Magnetic field dependence of (b) q and (c) $P_{[110]}$ (with two kinds of H-sweeping rates for process [ii]) at 2 K in $CuFeO_2$. (d) Measurement paths on the H-T phase diagram for $CuFe_{0.98}Al_{0.02}O_2$. Wavy lines denote that electric field is applied. Magnetic field dependence of (e) q and (f) $P_{[110]}$ at 2 K in $CuFe_{0.98}Al_{0.02}O_2$. The data for (a) are taken from Ref. [12], and the data for (d) and (e) are taken from Ref. [25].

III. RESULTS AND DISCUSSION

A. An irreversible H evolution of P induced by H sweeping under applied E

1. Importance of the H variation of an incommensurate wave number q in the phenomenon

Process [i] in Fig. 3(c) shows the H dependence of $P_{[110]}$ measured by increasing or decreasing H from 10 T at 2 K. Before the measurement, a poling electric field E_p of 800 kV/m was applied typically at 16 K on cooling, which is well above the ferroelectric phase-transition temperature of ~9 K, and was removed at 2 K, as shown in Fig. 3(a), process [i]. Hereafter, we refer to the application of E_p through the phase transition as proper poling. By proper poling, we can obtain the macroscopic $P_{[110]}$ as a result of an imbalance of the helicity domain volume fraction. Here, we emphasize that this H dependence of $P_{[110]}$ is linear. On the other hand, when we apply E of 800 kV/m at 2 K (well below the phase-transition temperature) after cooling without E_p at 10 T, $P_{[110]}$ shows almost no macroscopic change and remains at 0 C/m^2. This indicates that the six multiferroic domain volume fractions do not change even when $E \sim 800$ kV/m is applied in the FE-ICM phase and the domain walls have a large coercive electric field. However, we have found a peculiar emergence of $P_{[110]}$ by H sweeping from 10 to 7 T with applied E of 800 kV/m, as shown by process [ii] in Figs. 3(a) and 3(c). Remarkably, when H is subsequently swept from 7 to 12 T under applied E, the $P_{[110]}$ that emerges irreversibly increases, instead of reversibly decreasing. For further H sweeping from 12 to 7 T, $P_{[110]}$ additively evolves.

To investigate the mechanism of this phenomenon, we have focused on the magnetic modulation wave number q in the FE-ICM phase as a physical quantity with H dependence [12] [see Fig. 3(b) [26]] and have performed similar experiments using CFAO. As shown in Figs. 3(d) and 3(e), CFAO exhibits the FE-ICM phase even under zero H [14,15], and q is almost field independent [25]. By proper poling, CFAO shows the same order of magnitude of $P_{[110]}$ in the FE-ICM phase as CFO [process [i] in Figs. 3(d) and 3(f)], whereas $P_{[110]}$ does not emerge by H sweeping under applied E, in contrast to CFO [process [ii] in Figs. 3(d) and 3(f)]. These results indicate that the H variation of q plays a key role in this phenomenon.

Thus, we have performed neutron diffraction experiments with *in situ* $P_{[110]}$ measurements to investigate the behavior of q in the H evolution of P. As shown in Figs. 2(b)–2(d), after the value of q was measured at 9 T [Fig. 2(d)], we swept H from 9 to 8.8 T [Fig. 2(b)] while measuring polarization currents [Fig. 2(c)]. Then, the value of q was measured again at 8.8 T, and subsequently, we again swept H from 8.8 to 8.6 T while measuring polarization currents. By step-by-step H sweeping in such a way, we obtained the H dependence of q and that of P, as shown in Fig. 2(d). As is clearly seen in Figs. 2(c) and 2(d), $P_{[110]}$ begins to increase when H starts to vary, and correspondingly, the value of q is slightly but notably changed before and after the H sweeping.

We have confirmed that the H dependence of q is the same under applied $E \neq 0$ or $E = 0$, as shown in Fig. 2(a). Note that the observed currents include the nuisance currents due to applied voltage of 800 V, as described in Sec. II B 1 [as indicated by red arrows in Fig. 2(c)], and thus, the accuracy of the absolute value of $P_{[110]}$ is limited [27].

2. The origin of this phenomenon among three factors for determining $P_{[110]}$

Here, we would like to identify the origin of this phenomenon among factors (i)–(iii) determining $P_{[110]}$, as described in Sec. I. In Figs. 4(a)–4(c), we show the H evolution of $P_{[110]}$, q, and the H dependence of integrated intensity under applied E, starting from the unpolarized state prepared by cooling down to 3 K at 10 T without E_p. For clarity in Figs. 4(a) and 4(d), we show the result of $P_{[110]}$ measured by continuously H sweeping, instead of the step-by-step H sweeping. Here, we have measured $P_{[110]}$ in off-bench experiments at HZB immediately after the neutron beam experiments, keeping the experimental setup at low T and restricting applied voltage to 400 V to avoid the nuisance current [28].

First, we think about factor (i), the q domain volume fractions. As shown in Figs. 4(c) and 4(f), the H dependence

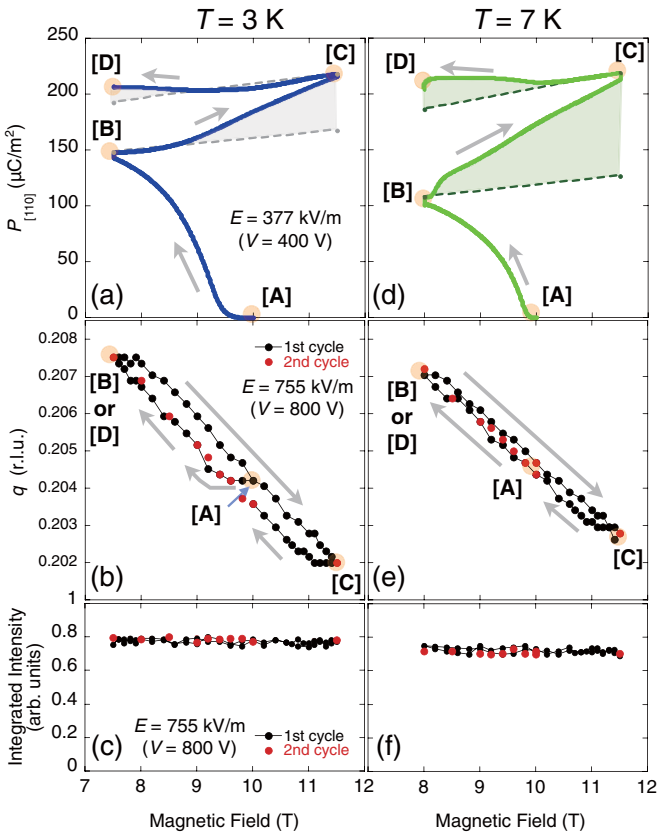

FIG. 4. H evolution of (a) $P_{[110]}$, (b) q, and (c) integrated intensity under applied E, starting from an unpolarized state prepared by cooling down to 3 K without E_p at 10 T. H evolution of (d) $P_{[110]}$, (e) q, and (c) integrated intensity under applied E at 7 K. Gray and green dashed lines are guidelines to demonstrate the H dependence of $P_{[110]}$ obtained by scaling the data measured with the proper-poling procedure (see text for details). The data for $P_{[110]}$ were obtained at HZB.

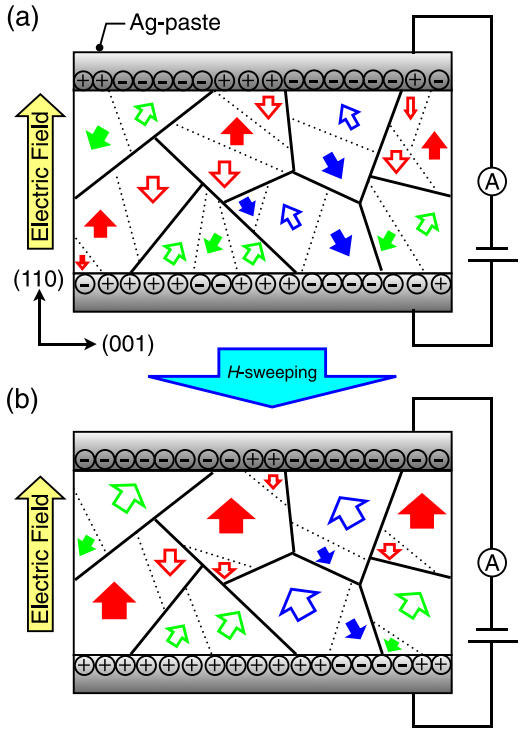

FIG. 5. Schematic illustration of (a) the macroscopic q domain and the helicity domain structures with P-induced charge on the electrode surfaces in the FE-ICM phase and (b) the q domain and the helicity domain structures after driving the helicity DWs by H sweeping and applied E. Solid (open) red, green, and blue arrows represent P induced by the left-handed (right-handed) helical magnetic order in the (110), $(\bar{2}10)$, and $(1\bar{2}0)$ domains, respectively. Solid lines and dashed lines denote the q domain walls and the helicity domain walls, respectively. Note that the size of the arrows denoting P has no meaning.

of the integrated intensity of the $(q-1,q,0.5)$ reflection does not change over several cycles of H sweeping even under applied E. Because an unpolarized neutron was used in this experiment, the helicity domain volume fractions cannot be discriminated from the magnetic reflections, which means that the integrated intensity of the $(q-1,q,0.5)$ reflection is proportional to one of the q domain volume fractions, namely, the (110) domain in this experimental setup. Thus, this result indicates that the q domain walls are not driven by H sweeping or by application of E, resulting in the q domain volume fractions not changing. Therefore, factor (i) is not the origin of the H evolution of $P_{[110]}$. Although the q domain volume fractions can be changed by H rotating within the ab plane, as reported by Seki *et al.* [21], the origin of this phenomenon is entirely different from the rearrangement of q domain structures.

Second, in order to consider a H variation of $P_{\rm local}$ [factor (iii)], let us recall the linear H dependence of $P_{[110]}$ obtained with the proper-poling procedure [Fig. 3(c), process [i]]. As reported by Nakajima *et al.* (see the inset in Fig. 10 in Ref. [29]), proper poling with applied $E_p \geqslant 600$ kV/m induces a saturation of P originating from an imbalance of the helicity domain volume fractions [factor (ii)] in $P-E_p$ curve. By proper poling, the helicity domain volume fractions are thus considered to be close to 1. Therefore, (also taking into account the fact that the q domain volume fractions do not change by H-sweeping), the linear H dependence of $P_{[110]}$ obtained by proper poling [Fig. 3(c), process [i]] is the H variation of $P_{\rm local}$ itself; $P_{\rm local}$ shows linear H dependence.

As is apparent from Figs. 4(a) and 4(d), however, the peculiar H evolution of $P_{[110]}$ is not explained by the linear H variation of $P_{\rm local}$. In the end, we have concluded that the nonlinear additive evolution of $P_{[110]}$ beyond the linear H variation of $P_{\rm local}$ is attributed to a change in the helicity domain volume fractions [factor (ii)], which would be achieved by driving the helicity DWs.

In Fig. 5, we schematically illustrate the q domain and the helicity domain structures in the FE-ICM phase during the H evolution of $P_{[110]}$. When the helicity DWs are driven by H sweeping under applied E, a ratio of the sign of the electric charges on the electrode surfaces is changed, as shown in Fig. 5(b). This would be the macroscopic picture on the H evolution of $P_{[110]}$.

3. *One-to-one correspondence between Δq and ΔP*

As mentioned above, the peculiarly irreversible H evolution of $P_{[110]}$ should include the H variation of $P_{\rm local}$ as the linear component, which is reversible. Therefore, there

should be an additive contribution of $P_{[110]}$ to the linear H variation of P_{local}. To demonstrate how the H evolution of $P_{[110]}$ includes the linear H variation of P_{local}, we plot gray dashed guidelines in Fig. 4(a). These guidelines represent the H dependence of $P_{[110]}$ expected by only the H variation of P_{local} in a process from point [B] to point [C] (or a process from point [C] to point [D]). As is clearly seen in the process from point [B] to point [C], $P_{[110]}$ follows the dashed line at the beginning and then starts to deviate from the dashed line upward and evolves additively.

In addition, corresponding to the behavior of $P_{[110]}$, q is almost constant for a while close to point [B] and then begins to vary, as shown in Fig. 4(b). Similarly, in the process from point [C] to point [D], $P_{[110]}$ decreases at the beginning instead of monotonically increasing, following the linear H variation of P_{local}, and then deviates from the dashed line and increases. This decreasing process of $P_{[110]}$ also indicates that this phenomenon is not due to a mere increment of trap charges on the electrode surfaces. Correspondingly, q is almost constant close to point [C] and then starts to change. Similar features are also seen in a process from point [A] to point [B]. Therefore, we have concluded that the variation of q (Δq) in H sweeping regardless of increasing or decreasing H is essential for the change in the helicity domain volume fractions by driving the helicity DWs, which produce the increment of P (ΔP) from the linear H variation of P_{local}. Furthermore, as shown in Figs. 4(d) and 4(e), the one-to-one correspondence between ΔP and Δq can also be seen at 7 K, although it is relatively incomprehensible compared with the results at 3 K.

Because $P_{[110]}$ shows remarkable T dependence at its emergence from the initially unpolarized state at 10 T, as shown in Fig. 6(a), we can check the one-to-one correspondence between $\Delta P_{[110]}$ and Δq. We refer to such a stage in H sweeping from 10 T (initially u-polarized state after cooling without applied E_p) to 9 T as the *initial* stage. In the initial stage, the change in q is expected to be small. Therefore, we used the $(2q,2q,0)$-second-harmonic reflections without E to accurately determine the H variation of q. Figure 6(c) shows the typical diffraction profiles at 10 and 9 T at 7 K and demonstrates that the H variation of $2q$ is visible despite the small intensity. Figure 6(b) shows the H dependence of Δq at several T. Both the H evolution of $P_{[110]}$ and the H dependence of Δq have a maximum at around 7 K. Moreover, both of them are smaller at 8.5 K than at 4 K. These results clearly demonstrate the qualitative one-to-one correspondence between $\Delta P_{[110]}$ and Δq. We have also confirmed that the q domain volume fractions are constant in H sweeping by measuring the intensities of the $(2q,2q,0)$, $(-4q,2q,0)$, and $(2q,-4q,0)$ reflections. They are unchanged over several cycles of H sweeping (not shown).

We expect that the H evolution of $P_{[110]}$ is independent of the H-sweep rate because the crucial factor for H evolution of $P_{[110]}$ is Δq. As shown in Fig. 3(c), we have observed that the H evolution of $P_{[110]}$ is not sensitive to the H-sweep rate in the range of 3.07 to 11.4 mT/s, as expected.

B. Role of H sweeping and applied E for the H evolution of P

Up to now, we have discussed the H evolution of $P_{[110]}$ for the case where we perform the H sweeping under simultaneously applied E. The role of E, however, may be driving the helicity DWs in general because they are ferroelectric. Then, taking into account the one-to-one correspondence between $\Delta P_{[110]}$ and Δq, we expect that Δq through H sweeping yields a movable state of the helicity DWs. To clarify this point, we have investigated the role of H sweeping for the H evolution of $P_{[110]}$ using the following procedure.

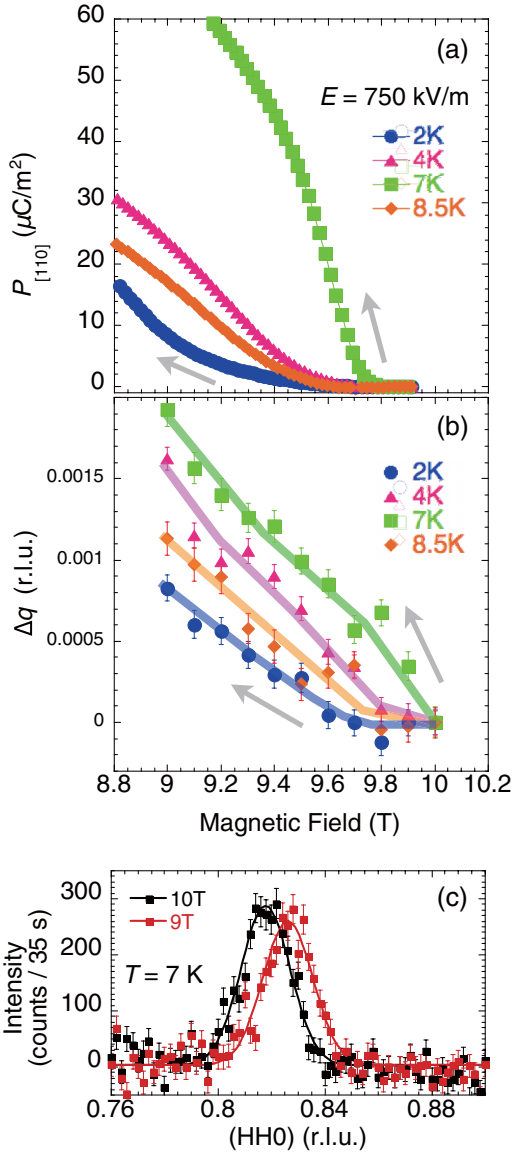

FIG. 6. H evolution of (a) $P_{[110]}$ and (b) difference in $q(H)$ from $q(10\text{ T})$ (Δq) at several temperatures below $T_{N2} \sim 9$ K after cooling at 10 T. The solid lines are guides for the eyes. (c) Typical diffraction profiles at 10 and 9 T at 7 K.

As illustrated in Fig. 7(a), in process (A), E was applied during H sweeping in the same way as before, after preparation of the initial state by cooling down to 7 K at 10 T without E_p. In process (B), on the other hand, E was not applied during H sweeping. After H sweeping from 10 to 9 T ($\Delta H = 1$ T), E was applied for 5 min at 9 T. Hereafter, we refer to $P_{[110]}$ induced by applying E after H sweeping in process (B) as $P^{\text{after}}_{[110]}$. It should be noted that $P^{\text{after}}_{[110]}$ cannot be estimated by time integration of the polarization current induced by applying E

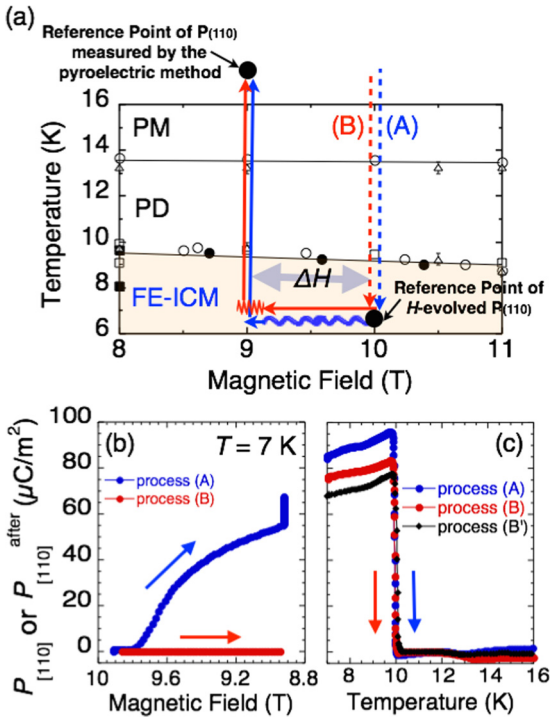

FIG. 7. (a) Measurement paths on the H-T phase diagram for CFO. Wavy lines denote that E is applied. (b) H evolutions of $P_{[110]}$. (c) T dependence of $P_{[110]}$ measured by the pyroelectric method in a heating run without applied E. In process (B′), indicated by the black diamonds in (c), we waited for 30 min after H sweeping from 10 to 9 T. Then, E was applied, and subsequently, $P^{\text{after}}_{[110]}$ was measured by the pyroelectric method in the heating run without applied E.

after H sweeping because huge currents (higher than signal polarization currents by two orders of magnitude) due to the sample behaving like a capacitor have flowed at application or removal of E at 9 T. Therefore, we have estimated $P^{\text{after}}_{[110]}$ using the pyroelectric method in a heating run without applied E.

Figure 7(b) shows the H evolution of $P_{[110]}$ in both processes. No emergence of $P_{[110]}$ was observed in process (B), indicating that E drives the DWs, as expected. Figure 7(c) shows the T dependence of $P_{[110]}$ in process (A) and $P^{\text{after}}_{[110]}$ in process (B) measured by the pyroelectric method in the heating run without applied E. $P^{\text{after}}_{[110]}$ at 7 K is comparable to $P_{[110]}$ at 7 K in process (A). This result indicates that the H variation of q yields a movable state of the helicity DWs and $P^{\text{after}}_{[110]}$ is induced by applying E after H sweeping via driving the helicity DWs. Therefore, simultaneous application of E and H sweeping is not necessary for this phenomenon; Δq through H sweeping cause the helicity DWs to be the movable state, and then E drives them.

Note that, as shown in Fig. 7(a), a reference point of the H-evolved $P_{[110]}$ in the time-integration process is at 10 T and 7 K in the FE-ICM phase immediately after cooling, whereas that of $P_{[110]}$ and $P^{\text{after}}_{[110]}$ measured with the pyroelectric method in the heating run is at 9 T and 18 K in the PM (PE) phase. As shown in Figs. 7(b) and 7(c), the value of $P_{[110]}$ measured by the pyroelectric method in process (A) is almost equivalent to that of H-evolved $P_{[110]}$ in process (A), despite different reference points. This result validates that we can compare the values of $P_{[110]}$ and $P^{\text{after}}_{[110]}$ with different reference points and that application or removal of E does not affect the value of $P_{[110]}$ or $P^{\text{after}}_{[110]}$.

Furthermore, we obtained a distinctive result which suggests that the ferroelectric helicity DWs are not simply dragged by the applied electric field. In process (B′), after preparation of the initial state by cooling down to 7 K at 10 T without E_p, we performed H sweeping from 10 to 9 T without applied E at 7 K, which is the same as process (B) to this point. Then, we waited for 30 min before E was applied for 5 min at 9 T. Subsequently, we measured the pyroelectric current in the heating run without applied E as in process (B). As a result, we found the same order of $P^{\text{after}}_{[110]}$, as shown in Fig. 7(c) [process (B′)]. This result suggests that the movable state of the helicity DWs is conserved for a while after H sweeping.

C. Speculation for microscopic helicity domain wall motion

The following two findings particularly suggest that microscopic helicity DW motion is not simple, compared with the usual ferroelectric domain-wall motion, in which the DWs are simply dragged by the applied electric field conjugating to the ferroelectric polarization:

(1) The value of evolved $P_{[110]}$ is determined by Δq (Sec. III A 3).

(2) After H sweeping without applied E, the movable state of the helicity DWs is conserved over several tens of minutes until E is applied (Sec. III B).

These findings suggest that Δq in H sweeping changes the state of the helicity domains and the helicity DWs. In the conventional DWs in Heisenberg ferromagnets, magnetic moments gradually rotate like a Bloch wall to locally minimize the energy loss of ferromagnetic exchange interaction between neighbor spins. In the case of the helicity DWs in the FE-ICM phase, in contrast, it may be relatively difficult to achieve the local energy minimization between neighbor spins around the helicity DW because the changeover from one helicity domain to the other helicity domain by gradual rotation is impossible [Fig. 8(a), graph (I)]. In H sweeping, Δq would cause the magnetic moments to have a global rotation so as to uniformly change a relative angle by the amount of $2\pi\Delta q$ between neighbor spins. If boundaries of the helical arrangement are open, the change in relative angle would be easily achieved. In the helical spin arrangement in the FE-ICM phase, however, the helicity DWs would work as a "pinning center" for the global rotations due to the impossible changeover of helicity at the helicity DWs. Thus, the helicity DWs would prevent the magnetic moments in the neighborhood of the helicity DWs from achieving the change in relative angle. As a result, the global rotations should mainly affect the neighborhood of the helicity DWs. Taking into consideration the difficulty of the local energy minimization around the helicity DW, these affected regions around the helicity DWs would store an extra exchange energy as a "twist" due to the global rotations. From finding 1, we expect that the affected region volume is proportional to Δq to a certain extent.

Here, we consider how much the global rotation affects the neighborhood of the helicity DWs using neutron diffraction profiles. There would be an extreme case in which the affected regions are perfectly disordered by the global rotation. In this

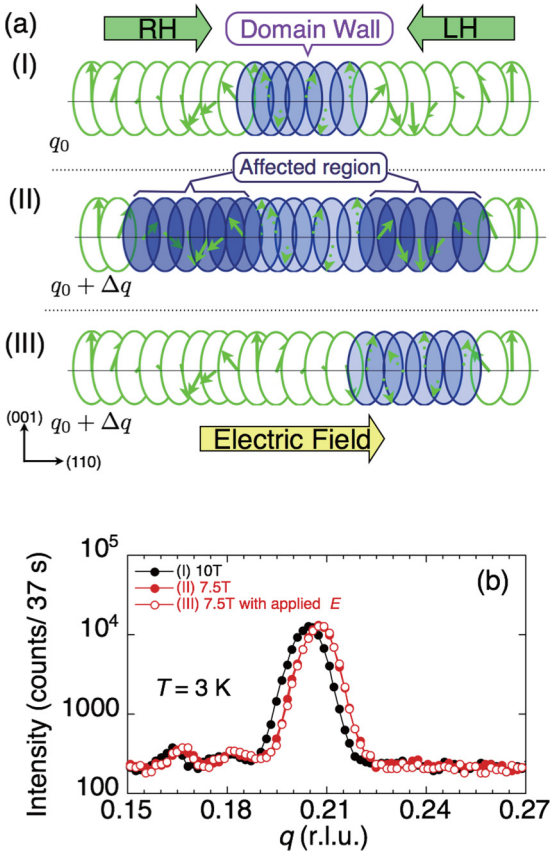

FIG. 8. (a) Schematic illustration of the helicity DW separating right-handed (RH) and left-handed (LH) helicity domains. (I) Unpolarized state immediately after cooling without E_p. The blue shaded area demonstrates the helicity DW. (II) By the global rotations, the extra exchange energy would be stored in the affected region. Dark shaded areas demonstrate the affected regions. (III) Then, applied E merges the affected regions and the helicity DWs into the helicity domain favored by the direction of E. (b) Typical diffraction profiles on a logarithmic scale at 10 or 7.5 T with or without applied E. (I)–(III) correspond to the domain states illustrated in (a).

case, a reduction of the fundamental magnetic Bragg reflection should be detected because the helicity domain volume is reduced due to the (disordered) affected region. As shown in Fig. 2(a) (the diffraction profiles for the presence and absence of the affected region should correspond to the profile at 7.5 T without and with E, respectively), however, the reduction of the intensity is not observed within the accuracy of this experiment. This result indicates that the affected regions are not perfectly disordered.

Similarly, it is possible that the affected regions have some short-range order, which should give rise to diffusive scattering superposed on the fundamental magnetic Bragg reflection with q. Figure 8(b) shows typical diffraction profiles on a logarithmic scale at 10 or 7.5 T with or without applied E. The diffusive scattering is not observed. Therefore, we have finding 3:

(3) The affected regions retain the original helical correlation.

Taking into account the distinctive findings 1–3, we have considered a scenario for the helicity DW movement as follows: the global rotations generate the affected regions, whose volume should be proportional to Δq to a certain extent, while the affected regions retain the original helical correlation [Fig. 8(a), graph (II)]. Because the affected regions store the extra exchange energy as a twist, they become metastable states. Then, applied E turns the metastable state into the lower-energy state so as to enlarge the helicity domain favored by the direction of E [Fig. 8(a), graph (III)], resulting in achievement of the helicity DW movement.

Although this speculation is in agreement with the distinctive findings 1–3, it does not indicate why the helicity DWs become sensible for E through the stored extra exchange energy as a twist and how the helicity DWs move. To establish this speculation as a model, direct observation of the helicity DW motion process and theoretical calculation of the helicity DW motion based on the microscopic spin dynamics in the affected region are highly desirable.

Here, we show the H evolution of $P_{[110]}$ over several cycles of H sweeping under applied E of 600 kV/m at 2, 7, and 8.5 K in Figs. 9(a)–9(c) [30], which would be compatible with our speculation of the helicity DW motion. In an *early* stage of up to a quarter cycle of H sweeping beyond the initial stage, we have found that overall H evolution of $P_{[110]}$ is almost the same, although we can see the remarkable T dependence of $P_{[110]}$ corresponding to the H variation of q in the initial stage, as shown in Fig. 6(b). In a *late* stage over several cycles of H sweeping, in contrast, the induced value of $P_{[110]}$ clearly depends on T: $P_{[110]}$ in the late stage at 2 K is almost saturated at less than half of the value obtained by proper poling. With increasing T, $P_{[110]}$ in the late stage increases toward the value obtained by proper poling. Especially at 8.5 K, it is comparable to the value obtained by proper poling.

As shown in Figs. 4(b) and 4(e), the overall trajectories of $q(H)$ at 2 and 7 K are almost the same except for the initial stage. Moreover, the trajectory of $q(H)$ over several cycles of H sweeping is unchanged. Therefore, recalling that Δq leads to the increment of $P_{[110]}$, we expect that $P_{[110]}$ should keep on increasing in the late stage over several cycles of H sweeping under applied E at any T so as to realize the single-helicity domain state. In spite of this expectation, the result shown in Fig. 9(a) indicates that some suppression factor exists which prevents the helicity DWs from further movement. Thermal fluctuation, however, may assist in driving the helicity DWs, and thus, especially at 8.5 K, the nearly single helicity domain state is realized. Based on our speculation, we would reasonably account for these results as follows: In the accumulation of the generation/consumption of the affected regions by several cycles of H sweeping under applied E, we can consider that the affected regions partially remain without being driven and behave as a "defect" preventing the helicity DWs from further movement. If the domain walls are simply dragged by external fields, such an accumulation process would be not expected.

Finally, we emphasize the following two points. First, what we have controlled is not the nuclei growth of one of the helicity domains by applied E on the ferroelectric transition [22] but the rearrangement of the helicity domain structures by driving the helicity DWs. Note that the helicity DWs in the FE-ICM phase are not originally driven by only applied E due to the large coercive electric field. Besides providing a

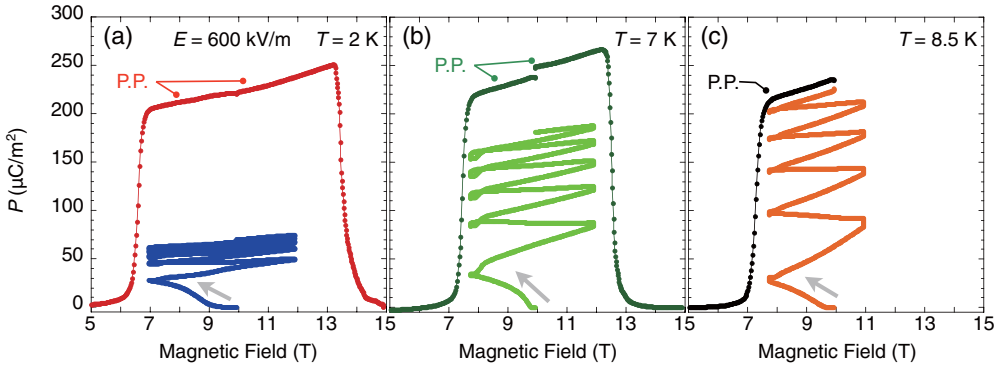

FIG. 9. H evolution of $P_{[110]}$ over several cycles of H sweeping under applied E at (a) 2 K, (b) 7 K, and (c) 8.5 K. For comparison, the H dependence of $P_{[110]}$ measured with the proper-poling (P.P.) procedure is also plotted.

technique for controlling the helicity DW in CFO systems, the control of the helicity domain in the present study is expected to be realized in other spin-driven ferroelectric materials with a large coercive electric field in a multiferroic phase. Second, the present study is nothing less than the achievement of driving the antiferromagnetic DW as well as that of driving the frozen ferroelectric DW even at 2 K. As Kagawa *et al.* have pointed out [9], in conventional antiferromagnets with a magnetic order of the magnetic modulation wave vector $\boldsymbol{Q}$, it is difficult to experimentally drive antiferromagnetic DWs because that requires spatially modulated magnetic field matching $\boldsymbol{Q}$. In contrast, we can easily drive antiferromagnetic DWs in multiferroics by applying a uniform electric field through the cross correlation between antiferromagnetism and ferroelectricity. Therefore, multiferroics also provide a good opportunity to investigate antiferromagnetic DWs and their dynamics.

IV. SUMMARY

We have found a peculiar irreversible evolution of $P_{[110]}$ by H sweeping under applied E in the FE-ICM phase of a spin-driven ferroelectric CFO, despite the large coercive electric field above 1 MV/m in this phase. Using neutron diffraction experiments with *in situ* $P_{[110]}$ measurements and the off-bench P measurements, we have revealed that the variation of q, Δq, in H sweeping regardless of increasing or decreasing H leads to the increment of $P_{[110]}$, which is achieved by the change in the helicity domain volume fractions by driving the helicity DW. From the further off-bench $P_{[110]}$ measurements, we have specified the role of H sweeping and applied E: Δq by H sweeping yields a movable state of the helicity DWs, and applied E drives them.

Based on these results, we have considered a scenario for the helicity DW movement: The variation of q would generate the affected regions, which may store the extra exchange energy as a twist and should be the metastable state, while the affected regions retain the original helical correlation. Then, applied E turns the metastable state into the lower-energy state as the helicity domain favored by the direction of E increases, resulting in the achievement of the helicity DW movement. To establish our speculation, further study of helicity DW dynamics, direct observation of the helicity DW motion process, and theoretical calculation of the helicity DW motion based on the microscopic spin dynamics in the helicity DWs are highly desirable.

The present study demonstrates the magnetoelectric cross correlation in driving the multiferroic DW: we could activate the frozen ferroelectric DW with the assistance of H sweeping, which is expected to be realized in other spin-driven ferroelectric materials as well. This is also an achievement of driving antiferromagnetic DW by applied uniform E, which is difficult in conventional antiferromagnets in principle.

ACKNOWLEDGMENTS

We thank the late group leader of the Nano Physics Group (NIMS), T. Takamasu, for pyroelectric measurements using the 15-T magnet at NIMS in the early stage of our study. We also thank HZB for the allocation of neutron beam time. The neutron diffraction experiments at HZB were carried out according to Proposals No. PHY-01-2963 and No. PHY-01-3270. This work was supported by a Grant-in-Aid for Scientific Research (C) (Grants No. 23540424 and No. 26400369) from the Japan Society for the Promotion of Science.

[1] T. Kimura, T. Goto, H. Shintani, K. Ishizaka, T. Arima, and Y. Tokura, Nature (London) **426**, 55 (2003).
[2] W. Eerenstein, N. D. Mathur, and J. F. Scott, Nature (London) **442**, 759 (2006).
[3] T. Kimura and Y. Tokura, J. Phys. Condens. Matter **20**, 434204 (2008).
[4] Y. Tokura and S. Seki, Adv. Mater. **22**, 1554 (2010).
[5] H. Katsura, N. Nagaosa, and A. V. Balatsky, Phys. Rev. Lett. **95**, 057205 (2005).
[6] C. Jia, S. Onoda, N. Nagaosa, and J. H. Han, Phys. Rev. B **76**, 144424 (2007).
[7] T. Arima, J. Phys. Soc. Jpn. **76**, 073702 (2007).

[8] F. Kagawa, M. Mochizuki, Y. Onose, H. Murakawa, Y. Kaneko, N. Furukawa, and Y. Tokura, Phys. Rev. Lett. **102**, 057604 (2009).

[9] F. Kagawa, Y. Onose, Y. Kaneko, and Y. Tokura, Phys. Rev. B **83**, 054413 (2011).

[10] M. Gajek, M. Bibes, S. Fusil, K. Bouzehouane, J. Fontcuberta, A. Barthelemy, and A. Fert, Nat. Mater. **6**, 296 (2007).

[11] S. Mitsuda, N. Kasahara, T. Uno, and M. Mase, J. Phys. Soc. Jpn. **67**, 4026 (1998).

[12] S. Mitsuda, M. Mase, K. Prokes, H. Kitazawa, and H. A. Katori, J. Phys. Soc. Jpn. **69**, 3513 (2000).

[13] T. Nakajima, S. Mitsuda, S. Kanetsuki, K. Prokes, A. Podlesnyak, H. Kimura, and Y. Noda, J. Phys. Soc. Jpn. **76**, 043709 (2007).

[14] S. Seki, Y. Yamasaki, Y. Shiomi, S. Iguchi, Y. Onose, and Y. Tokura, Phys. Rev. B **75**, 100403(R) (2007).

[15] S. Kanetsuki, S. Mitsuda, T. Nakajima, D. Anazawa, H. A. Katori, and K. Prokes, J. Phys. Condens. Matter **19**, 145244 (2007).

[16] N. Terada, T. Nakajima, S. Mitsuda, H. Kitazawa, K. Kaneko, and N. Metoki, Phys. Rev. B **78**, 014101 (2008).

[17] E. Pachoud, C. Martina, B. Kundys, C. Simona, and A. Maignana, J. Solid State Chem. **183**, 344 (2010).

[18] T. Kimura, J. C. Lashley, and A. P. Ramirez, Phys. Rev. B **73**, 220401(R) (2006).

[19] T. Nakajima, S. Mitsuda, S. Kanetsuki, K. Tanaka, K. Fujii, N. Terada, M. Soda, M. Matsuura, and K. Hirota, Phys. Rev. B **77**, 052401 (2008).

[20] T. Nakajima, S. Mitsuda, T. Nakamura, H. Ishii, T. Haku, Y. Honma, M. Kosaka, N. Aso, and Y. Uwatoko, Phys. Rev. B **83**, 220101 (2011).

[21] S. Seki, H. Murakawa, Y. Onose, and Y. Tokura, Phys. Rev. Lett. **103**, 237601 (2009).

[22] T. Nakajima, S. Mitsuda, K. Takahashi, H. Yamazaki, K. Yoshitomi, M. Soda, M. Matsuura, and K. Hirota, Phys. Rev. B **82**, 064418 (2010).

[23] T. R. Zhao, M. Hasegawa, and H. Takei, J. Cryst. Growth **166**, 408 (1996).

[24] Note that the $(\bar{1},0,\bar{1})+(q,q,3/2)$ magnetic Bragg point belongs to the (110) domain. Moreover, $P_{[110]}$ measured in this experiment is mainly attributed to P in the (110) domain because the poling electric field contributes only half to the $(\bar{2}10)$ or $(1\bar{2}0)$ domain due to the [110] electrodes, and also, P in the $(\bar{2}10)$ or $(1\bar{2}0)$ domain contributes only half to $P_{[110]}$, as described in Sec. I. Therefore, this reflection is suitable for simultaneous measurements of q and $P_{[110]}$.

[25] N. Terada, S. Mitsuda, K. Prokeš, O. Suzuki, H. Kitazawa, and H. A. Katori, Phys. Rev. B **70**, 174412 (2004).

[26] For clarity, we present the data obtained by $2q$ measurements in this work in Fig. 3(b) because the data for H dependence of q reported by Mitsuda *et al.* [12] was measured at 7 K and across the phase boundary between the FE-ICM phase and the 5SL phase.

[27] In addition, we measured the polarization current only in the middle of H sweeping, and thus, we did not obtain the current data during each measurement of q. Moreover, even after stopping H sweeping, $P_{[110]}$ gradually increases through a relaxation process. Therefore, the absolute value of $P_{[110]}$ is not accurately determined by these *in situ* measurements with the step-by-step H sweeping. See Supplemental Material at http://link.aps.org/supplemental/10.1103/PhysRevB.93.174101 for detailed results of the relaxation process.

[28] We have confirmed that the overall H evolution of $P_{[110]}$ measured by the continuous H sweeping is intrinsically equivalent to one measured by the step-by-step H sweeping. See the Supplemental Material for a comparison.

[29] T. Nakajima, S. Mitsuda, K. Takahashi, M. Yamano, K. Masuda, H. Yamazaki, K. Prokes, K. Kiefer, S. Gerischer, N. Terada, H. Kitazawa, M. Matsuda, K. Kakurai, H. Kimura, Y. Noda, M. Soda, M. Matsuura, and K. Hirota, Phys. Rev. B **79**, 214423 (2009).

[30] As reported by Nakajima *et al.* [20] and Mitsuda *et al.* [31], the q domain volume fraction is easily changed by applying only 5–10 MPa of uniaxial pressure at room temperature. Therefore, the reason why the value of $P_{[110]}$ at 2 K in Fig. 9(a) is different from that of $P_{[110]}$ at 2 K in Fig. 3(c) is attributed to the difference of not the magnitude of applied E but the q domain volume fraction owing to a slight difference in the sample mounting with varnish. Within the same experiment period, however, the value of $P_{[110]}$ is reproducible, and thus, it is considered that the q domain volume fraction is unchanged.

[31] S. Mitsuda, K. Yoshitomi, T. Nakajima, C. Kaneko, H. Yamazaki, M. Kosaka, N. Aso, Y. Uwatoko, Y. Noda, M. Matsuura, N. Terada, S. Wakimoto, M. Takeda, and K. Kakurai, J. Phys. Conf. Ser. **340**, 012062 (2012).